Article

The Effect of Bi Addition on the Electromigration Properties of Sn-3.0Ag-0.5Cu Lead-Free Solder

Huihui Zhang [1], Zhefeng Xu [1,2,*], Yan Wang [1], Caili Tian [3], Changzeng Fan [1,2], Satoshi Motozuka [4] and Jinku Yu [1]

1 State Key Laboratory of Metastable Materials Preparation Technology and Science, Yanshan University, Qinhuangdao 066004, China; huihuizhang0809@163.com (H.Z.)
2 Hebei Province Comprehensive Optimization Laboratory of Metal Products Technology and Properties, Yanshan University, Qinhuangdao 066004, China
3 Institute of Energy Resources, Hebei Academy of Sciences, Shijiazhuang 050081, China
4 Graduate School of Advanced Science and Technology, Hiroshima University, Higashi-Hiroshima 739-8527, Japan
* Correspondence: zfxu@ysu.edu.cn

Abstract: As electronic packaging technology advances towards miniaturization and integration, the issue of electromigration (EM) in lead-free solder joints has become a significant factor affecting solder joint reliability. In this study, a Sn-3.0Ag-0.5Cu (SAC305) alloy was used as the base, and different Bi content alloys, SAC305-*x*Bi (x = 0, 0.5, 0.75, 1.0 wt.%), were prepared for tensile strength, hardness, and wetting tests. Copper wire was used to prepare EM test samples, which were subjected to EM tests at a current density of approximately 0.6×10^4 A/cm^2 for varying durations. The interface microstructure of the SAC305-*x*Bi alloys after the EM test was observed using an optical microscope. The results showed that the 0.5 wt.% Bi alloy exhibited the highest ultimate tensile strength and microhardness, improving by 33.3% and 11.8% compared to SAC305, respectively, with similar fracture strain. This alloy also displayed enhanced wettability. EM tests revealed the formation of Cu_6Sn_5 and Cu_3Sn intermetallic compounds (IMCs) at both the cathode and anode interfaces of the solder alloy. The addition of Bi inhibited the diffusion rate of Sn in Cu_6Sn_5, resulting in similar total IMC thickness at the anode interface across different Bi contents under the same test conditions. However, the total IMC thickness at the cathode interface decreased and stabilized with increasing EM time, with the SAC305-0.75Bi alloy demonstrating the best resistance to EM.

Keywords: lead-free solder; SAC305; Bi; electromigration; mechanical properties; wettability

Citation: Zhang, H.; Xu, Z.; Wang, Y.; Tian, C.; Fan, C.; Motozuka, S.; Yu, J. The Effect of Bi Addition on the Electromigration Properties of Sn-3.0Ag-0.5Cu Lead-Free Solder. *Metals* **2024**, *14*, 1149. https://doi.org/10.3390/met14101149

Received: 6 September 2024
Revised: 2 October 2024
Accepted: 3 October 2024
Published: 8 October 2024

Copyright: © 2024 by the authors. Licensee MDPI, Basel, Switzerland. This article is an open access article distributed under the terms and conditions of the Creative Commons Attribution (CC BY) license (https://creativecommons.org/licenses/by/4.0/).

1. Introduction

The traditional Pb-Sn solder has been restricted for use due to its environmental and human health hazards, making the development and application of lead-free solder a major trend. In recent years, the focus of research on low-temperature lead-free solder has primarily focused on tin-based lead-free solders, including Sn-Ag [1], Sn-Cu [2], Sn-Zn [3], Sn-Bi [4], Sn-Ag-Cu [5], etc. Among these, the Sn-3.0Ag-0.5Cu (SAC305) lead-free solder, recommended by the Japan Electronics and Information Technology Industries Association (JEITA), is one of the most representative lead-free solder alloys in the current market [6].

With the gradual development of electronic packaging technology towards miniaturization and high integration, the spacing and size of each solder joint have decreased, leading to an increase in current density within the solder joint [7]. As a result, the phenomenon of electromigration (EM) at the solder joint interface becomes more pronounced (As shown in Figure 1), making it prone to failure and significantly reducing the service life of electronic products. Therefore, it is necessary to research lead-free solders with better EM reliability.

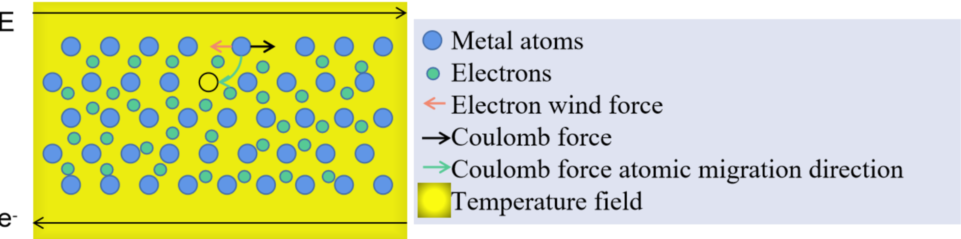

Figure 1. Schematic diagram of electromigration.

The current measures to mitigate the harmful effects of EM mainly involve the addition of trace alloying elements, doping with nanoparticles [8,9], or controlling current density [10–16]. Incorporating suitable alloying elements or doping with nanoparticles can enhance the resistance of solder joints to EM, thereby improving their reliability. Ma et al. [10] investigated the influence of Co addition on the EM performance of Sn-3.0Ag-0.5Cu solder, confirming that the addition of Co effectively suppressed the formation of needle-like and plate-like Cu_6Sn_5 intermetallic compounds (IMCs), refined the microstructure, and significantly enhanced the reliability of the solder joints. Bashir M. et al. [11] studied the effect of Zn nanoparticle doping on the EM performance of SAC305 and found that the addition of 2 wt.% Zn suppressed the formation of voids and cracks at the cathode interface and controlled the growth rate of IMCs at the anode interface. Youngseok Kim et al. [12] investigated the effect of Co and Ni addition on the EM performance of Sn-Ag-Bi-In alloy. They found that the addition of Co and Ni refined the grain structure, inhibited Cu dissolution, and controlled IMC growth affected by grain boundary interference, thereby improving the EM performance of Sn-Ag-Bi-In alloy.

Sun et al. [13] investigated the effects of Bi and Ni on the EM performance of Sn-0.7Ag-0.5Cu solder joints. They found that the addition of Bi and Ni lowered the melting point of the Sn-0.7Ag-0.5Cu solder, improved its wetting with the Cu substrate, reduced the grain size of IMCs, and enhanced EM performance. Wang et al. [14] studied the influence of Cu on the EM performance of Sn-Ag eutectic solder joints. They observed a significant reduction in the growth of anode interface IMCs in the solder joints when the Cu content was 2 wt.%, effectively mitigating the harmful effects of EM. Liang et al. [15], while studying the effects of current density and Joule heating on EM, found that appropriately reducing the current density can mitigate the detrimental effects of EM. Additionally, Wang et al. [16] deposited a Ni/Ag (1 µm/1.5 µm) barrier layer on the solder pad above the solder joint. During the EM process, this layer formed a thin layer of Ag_3Sn serving as a barrier to suppress current-induced Cu dissolution, thereby significantly improving the reliability of the solder joint.

The addition of Bi can lower the melting point of SAC305 solder and increase its wettability on Cu substrates [17]. However, the existing research only focuses on the effects of high Bi content on the mechanical properties and wettability of SAC305. There have been no reports on the impact of Bi addition on the EM performance of SAC305 solder. Therefore, this study aims to add different amounts of Bi to SAC305 through micro-alloying. On the one hand, it investigates the influence of trace Bi on its mechanical properties and wettability; on the other hand, it seeks to confirm whether it can have a positive effect on the EM performance of SAC305 solder and inhibit EM failure behavior. This is of significant importance for improving the EM resistance of SAC305.

2. Materials and Methods

The experimental materials used in this study are the widely used lead-free solder Sn-3.0Ag-0.5Cu and high-purity (99.99%) Bi. A certain mass ratio of SAC305 solder and pure Bi was melted and cast into a mold to obtain lead-free solder alloys SAC305-xBi (x = 0, 0.5, 0.75, 1.0 wt.%) upon cooling in the mold (as shown in Figure 2). The melting temperature for the material casting process is 500 °C. During this period, the mold is

heated together with the material. Once the composition of the molten metal is uniform, it is poured into the mold and allowed to cool naturally at room temperature.

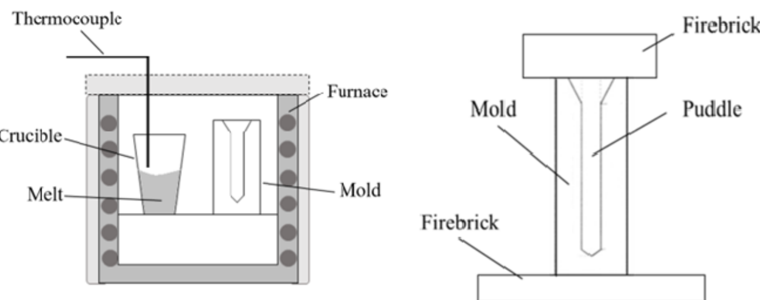

Figure 2. Schematic diagram of material casting.

The SAC305-xBi solder castings were machined to obtain cylindrical tensile samples, as shown in Figure 3. Tensile tests were conducted using a computer-controlled universal testing machine (WDW-50E, the equipment comes from Jinan, Shandong, China) at a strain rate of 0.02 mm/min, and the tensile curves were subsequently analyzed. Additionally, hardness tests were performed using a Vickers hardness tester (FM-700, the equipment comes from FUTURE TECH in Tokyo, Japan) with a load of 50 gf and a dwell time of 10 s.

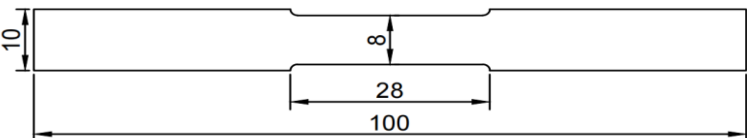

Figure 3. Schematic diagram of tensile samples (Units: mm).

A rosin alcohol solution containing 5 wt.% $ZnCl_2$ was used as a flux for solder wettability testing and the preparation of EM test specimens. For the wettability test, copper substrates with dimensions of 15 × 15 × 1 mm were used, with a solder amount of 100 mg. The copper substrates were polished and leveled using sandpaper, cleaned with a 5% (v/v) HCl solution, anhydrous ethanol, and deionized water, and then dried. Soldering was performed at 250 °C, and after the experiment, the spreading area and wetting angle of the solder were measured.

Copper wire with a diameter of 0.5 mm and 20 mg solder were used to prepare the sample for the EM experiment, maintaining a distance between the two copper wires of 1.1–1.3 mm. Before preparing the sample, the end faces of the copper wires were leveled, and both the wires and solder were cleaned using a 5% (v/v) HCl solution, anhydrous ethanol, and deionized water, and then dried. Subsequently, the EM test specimens were prepared using a mold on a heating platform at a soldering temperature of 250 °C.

The solder was subjected to EM experiments using the direct current power supply unit PWR801L over durations of 0, 24, 48, and 72 h. Chen et al. [18] found that the theoretical critical current density for interconnect leads in electronic packaging can approach 10^5 A/cm^2, while the actual critical current density in electronic packaging is around 10^4 A/cm^2. Considering the materials used in the experiment, a current of 12.2 A was applied, resulting in an interface current density of approximately 0.6×10^4 A/cm^2. Under these conditions, the samples meet the criteria for electromigration. Furthermore, the experiments will be conducted at room temperature to ensure that the heat generated by resistance at the solder joints can dissipate effectively, thereby reducing the impact of Joule heating on the experimental results. The microstructure of the solder–copper wire interface following the EM experiment was observed using an optical microscope, and the morphology and thickness changes in the IMC at the solder joint and copper interface were

analyzed. The impact of the Bi element on the EM performance of SAC305-*x*Bi solders was also analyzed.

3. Results and Discussion

3.1. Mechanical Property

Figure 4 displays the microhardness of the SAC305-*x*Bi alloys. It can be observed from the figure that the microhardness of the SAC305 alloy, without the addition of Bi element, measures 17.1 HV. The experimental results are close to the SAC305 hardness obtained by REN et al. [19]. As the Bi content increases, the microhardness of the SAC305-*x*Bi alloys shows an increasing trend, followed by a decline. However, the microhardness of the SAC305-*x*Bi alloys does not exhibit a significant decrease even with the addition of Bi.

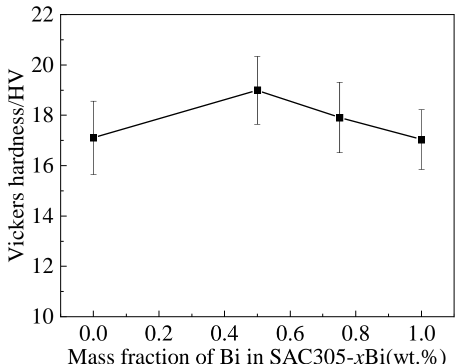

Figure 4. Vickers hardness of SAC305-*x*Bi alloys.

Figure 5 shows the stress–strain curve of SAC305-*x*Bi, while Figure 6 shows the variations in ultimate tensile strength and fracture strain across different Bi content. From Figures 5 and 6, it can be concluded that with the addition of Bi, the ultimate tensile strength of the SAC305 solder first increases and then decreases, while the fracture strain first decreases gradually and then decreases sharply. The ultimate tensile strength and fracture strain of the SAC305 alloy are about 37.5 MPa and 42.5%, respectively. The experimental results are similar to those measured by Tu et al. [20]

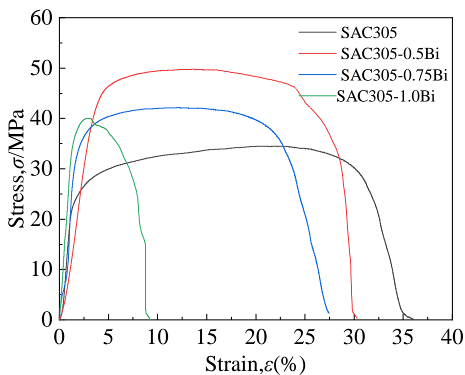

Figure 5. Stress–strain curves of SAC305-*x*Bi alloys.

The ultimate tensile strength of the SAC305 alloy is enhanced with the increase in Bi content. When the Bi content was 0.5%, the ultimate tensile strength of the alloy reached about 50 MPa. Moreover, the ultimate tensile strength of solder alloys with a Bi content of 0.75% and 1.0% both exceeded 40 MPa, which is higher than that of the SAC305 alloy. With the increase in Bi content, the fracture strain decreases sharply at 1.0% Bi content. However, the fracture strain of solder alloys with a Bi content of 0.5% and 0.75% is lower than that of SAC305, but they showed good plasticity.

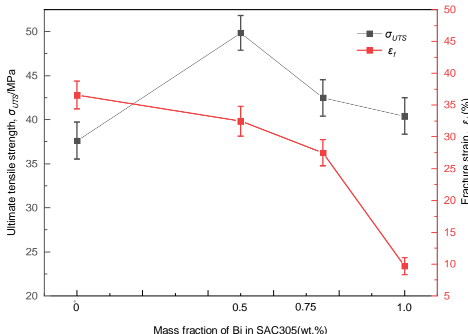

Figure 6. Ultimate tensile strength and fracture strain of SAC305-*x*Bi alloys.

3.2. Wettability of SAC305-xBi Alloys

The wetting properties of solder can be evaluated by the spreading area of the solder on the substrate and the contact angle [21,22]. Figure 7 shows the wetting performance of the SAC305-*x*Bi alloys on a Cu substrate. It can be observed that the addition of Bi element has improved the wetting properties of the alloy to a certain extent. The spreading area and contact angle of the alloy without Bi element are approximately 27 mm^2 and 52°, respectively. With the increase in Bi content, the spreading area of the solder alloy on the Cu substrate initially increases and then decreases, while the contact angle shows an initial decrease followed by an increase. When the Bi element content is 0.5 wt.%, the alloy exhibits the largest spreading area and the smallest contact angle, with improvements of 11.1% and 4.0%, respectively, compared to the SAC305 alloy. The wettability of lead-free solder is closely related to the surface tension during the soldering process. Generally, a smaller surface tension results in better wettability. The addition of Bi affects the formation of intermetallic compounds (IMCs) between the solder and the substrate, which in turn influences the surface tension. As the IMC thickness increases, the surface tension also increases, leading to poorer wettability. The alloy with 0.5% Bi forms the thinnest IMC layer, resulting in optimal wettability. The wettability of other alloy compositions also correlates with the thickness of the IMC. This phenomenon has also been observed by Qu et al. [23].

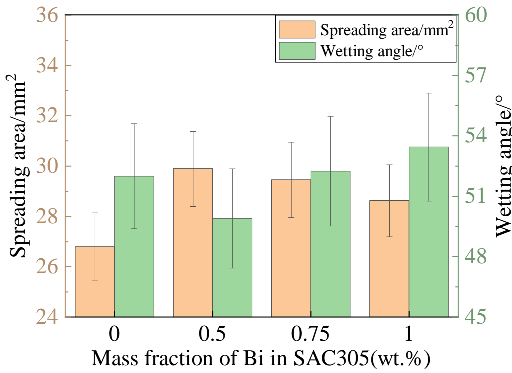

Figure 7. Wettability diagram of SAC305-*x*Bi alloys.

3.3. Electromigration Properties

During the EM process, in the SAC305 alloy, Cu atoms migrate from the cathode to the anode, causing the growth and thickening of the IMC on the anode side, while the thickness of the IMC on the cathode side decreases, accompanied by the appearance of voids and other defects [24]. Figure 8 shows the microstructure of the IMC at the interface after soldering the SAC305 alloy and copper wire. Through the EDS line scan data, it can be observed that two types of intermetallic compounds (IMCs) are formed at the soldering interface. According to the research by Chantaramanee, S. et al. [25] on the microstructure of the SAC305-*x*Bi and Cu interconnect interface, it can be determined that these two types of IMCs are Cu_6Sn_5 and Cu_3Sn, with Cu_3Sn in contact with the Cu side

and Cu_6Sn_5 in contact with the solder side. The study added Bi wt.% ≥ 1 wt.%, and the welding time was 2 min, which is longer than the 30 s used in this research. Therefore, when the Bi addition content is the same at 1 wt.%, the measured IMC thickness reported by Chantaramanee, S. et al. [25] is much greater than the results of this experiment.

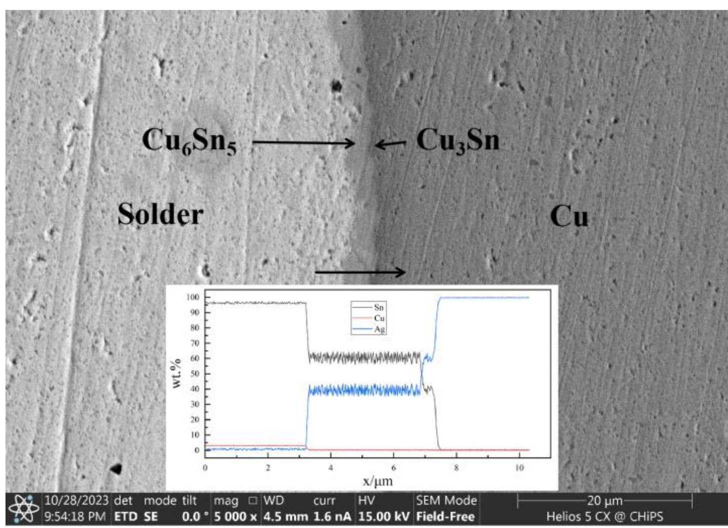

Figure 8. Microstructure of IMC at the interface between SAC305 alloy and copper wire after welding.

The effects of different EM experiment durations on SAC305-xBi are shown in Figures 9–12a–h, where Figures 9–12a–d depict the microstructure of the cathode interface IMC after 0 h, 24 h, 48 h, and 72 h of EM experiments, respectively, and Figures 9–12e–h show the microstructure of the anode interface IMC after 0 h, 24 h, 48 h, and 72 h of EM experiments, respectively. It can be observed that, after different durations of EM experiments, the total thickness of the IMC at the cathode interface of the SAC305 alloy decreased from 4.27 μm to 2.95 μm, 2.73 μm, and 2.65 μm, while the total thickness of the IMC at the anode interface increased from 4.27 μm to 4.42 μm, 4.76 μm, and 5.00 μm.

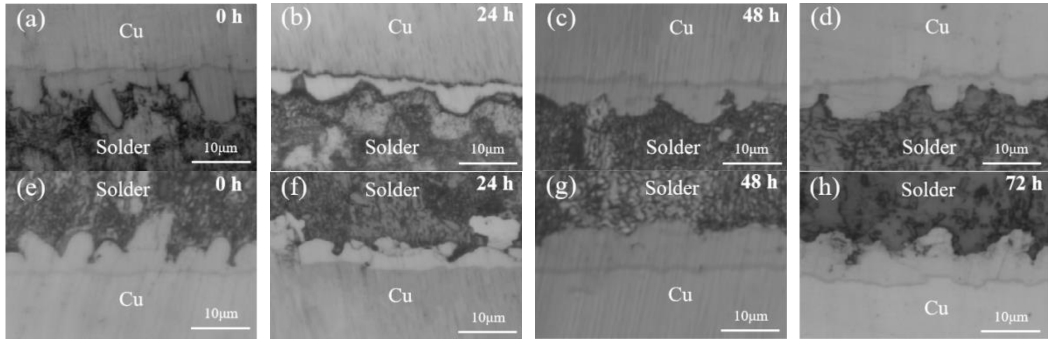

Figure 9. Interconnection interface microstructure of SAC305 alloy after EM test across different times. (**a**–**d**): Cathode; (**e**–**h**): anode; (**a**,**e**): 0 h; (**b**,**f**): 24 h; (**c**,**g**) 48 h; (**d**,**h**): 72 h.

As the Bi content increases, the total thickness of the IMC at the cathode interface of the SAC305-0.5Bi alloy decreased from 3.83 μm to 3.23 μm, 3.15 μm, and 2.74 μm across the different durations of EM experiments, while the total thickness of the IMC at the anode interface increased from 3.83 μm to 4.11 μm, 4.76 μm, and 4.84 μm. For the SAC305-0.75Bi alloy, the total thickness of the IMC at the cathode interface decreased from 4.14 μm to 4.11 μm, 4.05 μm, and 3.71 μm; at the anode interface, it increased from 4.14 μm to 4.32 μm, 4.84 μm, and 5.02 μm. In the case of the SAC305-1.0Bi alloy, the total thickness of the IMC at the cathode interface decreased from 4.00 μm to 3.62 μm, 3.39 μm, and 3.31 μm; while at the anode interface, it increased from 4.00 μm to 4.76 μm, 4.84 μm, and 5.05 μm.

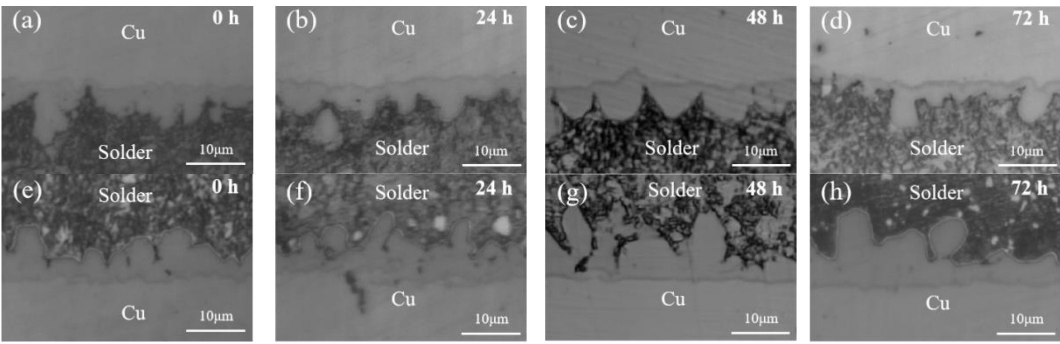

Figure 10. Interconnection interface microstructure of SAC305-0.5Bi alloy after EM test across different times. (**a**–**d**): Cathode; (**e**–**h**): anode; (**a**,**e**): 0 h; (**b**,**f**): 24 h; (**c**,**g**): 48 h; (**d**,**h**): 72 h.

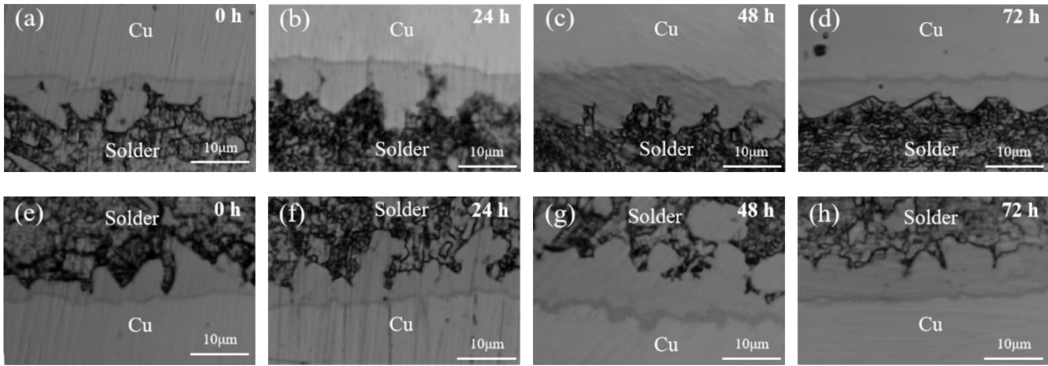

Figure 11. Interconnection interface microstructure of SAC305-0.75Bi alloy after EM test across different times. (**a**–**d**): Cathode; (**e**–**h**): anode; (**a**,**e**): 0 h; (**b**,**f**): 24 h; (**c**,**g**): 48 h; (**d**,**h**): 72 h.

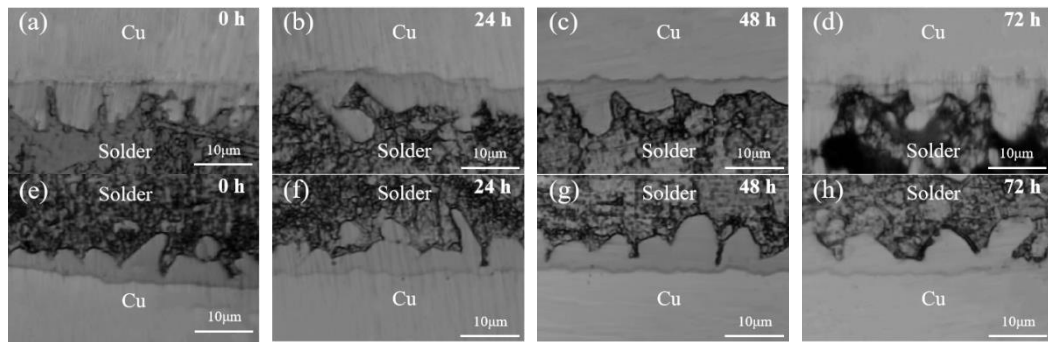

Figure 12. Interconnection interface microstructure of SAC305-1.0Bi alloys after EM test across different times. (**a**–**d**): Cathode; (**e**–**h**): anode; (**a**,**e**): 0 h; (**b**,**f**): 24 h; (**c**,**g**): 48 h; (**d**,**h**): 72 h.

The graph in Figure 13 represents the variation in the thickness of the IMC at the cathode and anode interfaces of SAC305-*x*Bi alloys after different durations of EM experiments. Before the EM experiments, the interface IMC thickness of the SAC305 solder was 4.27 μm. With an increase in the Bi element content, the total thickness of the interface IMC of the SAC305-*x*Bi alloys decreased. Specifically, the interface IMC total thickness corresponding to Bi element contents of 0.5 wt.%, 0.75 wt.%, and 1.0 wt.% was 3.83 μm, 4.14 μm, and 4.00 μm, respectively. These experimental results align with those reported by Chantaramanee, S. et al. [25], indicating that the addition of Bi reduces copper solubility and slows down the reaction rate between SAC305-*x*Bi alloys and Cu, thereby reducing the total thickness of interface IMC.

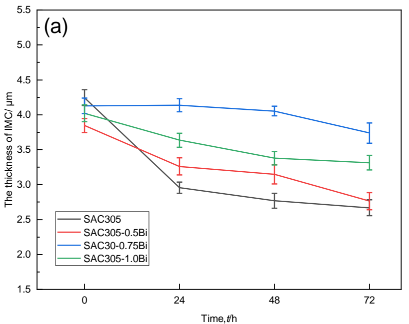

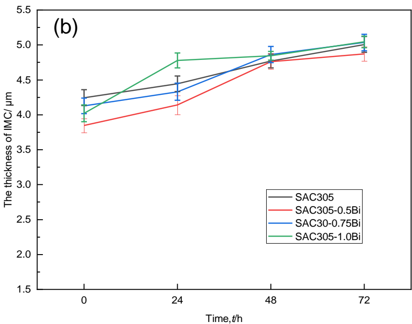

Figure 13. Change in IMC thickness at the interface of SAC305-*x*Bi alloys (**a**): cathode (**b**): anode.

Figure 13 depicts the variation in the total thickness of the IMC at the cathode and anode interfaces of SAC305-*x*Bi alloys over different EM durations. Figure 14 shows the changes in the thickness at the cathode and anode of the interface IMC of SAC305-*x*Bi alloys after 72 h of EM compared to SAC305. An analysis of the experimental data reveals that, for SAC305-*x*Bi alloys with different Bi contents, the growth rate of total IMC thickness at the anode interface after 72 h of EM is not particularly significant. However, the reduction in total IMC thickness at the cathode interface is noticeably inhibited, and the inhibitory effect varies with the Bi content. When the Bi element content is 0.75 wt.%, the total thickness of IMC at the cathode interface hardly decreases during the EM experiment, indicating a significant improvement in the EM performance.

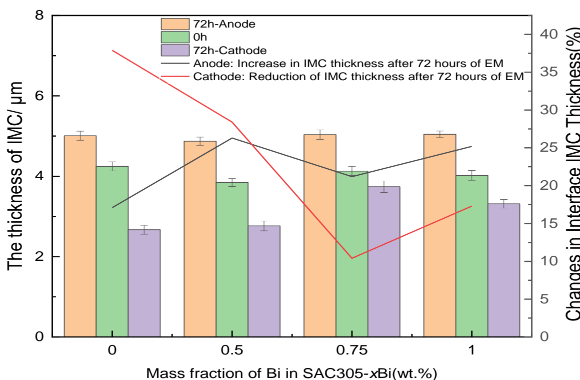

Figure 14. Interface IMC thickness change in SAC305-*x*Bi alloy after 72 h of EM.

During the soldering process, the Bi element in SAC305-*x*Bi alloys does not react with Cu atoms but only consumes Sn atoms, resulting in the interface IMC total thickness of the Bi-containing alloy being smaller than that of SAC305 before EM experiments [26]. When electromigration occurs at the solder joint, the Cu element migrates from the cathode to the anode under the influence of the current. This process causes the decomposition of Cu_6Sn_5 and Cu_3Sn on the cathode side, ultimately leading to a reduction in the thickness of the intermetallic compound (IMC) at the cathode. One of the fundamental factors affecting this process is the grain orientation. When the c-axis of the β-Sn grains is aligned with the direction of the current, the diffusion rate of Cu under the influence of the current is faster [27]. This is because the diffusion coefficient of Cu atoms along the c-axis of β-Sn grains is about 500 times that along the a-axis and b-axis [28]. Additionally, the Bi element, existing in solid solution within the SAC305 alloy, refines the β-Sn grains through solid solution strengthening. By increasing the orientation of Sn grains and the number of grain boundaries through this method, as shown in Figure 15, the distribution of angular γ between [001]Sn and the direction of the current is different at different points. The diffusion of Cu from the cathode to the anode can be suppressed, thereby reducing the decomposition of Cu_6Sn_5 and Cu_3Sn on the cathode side [29]. Furthermore, the addition of Bi inhibits the diffusion rate of Sn in Cu_6Sn_5 [30]. This results in a slower reduction in

the total thickness of the IMC at the cathode interface in Bi-containing alloys under the influence of current, with a smaller effect at the anode interface. When the Bi content reaches 1%, the EM resistance of the alloy diminishes, and the improvement in EM performance does not increase with the increase in Bi content. The mechanism behind this phenomenon has not been fully confirmed, and further research is needed.

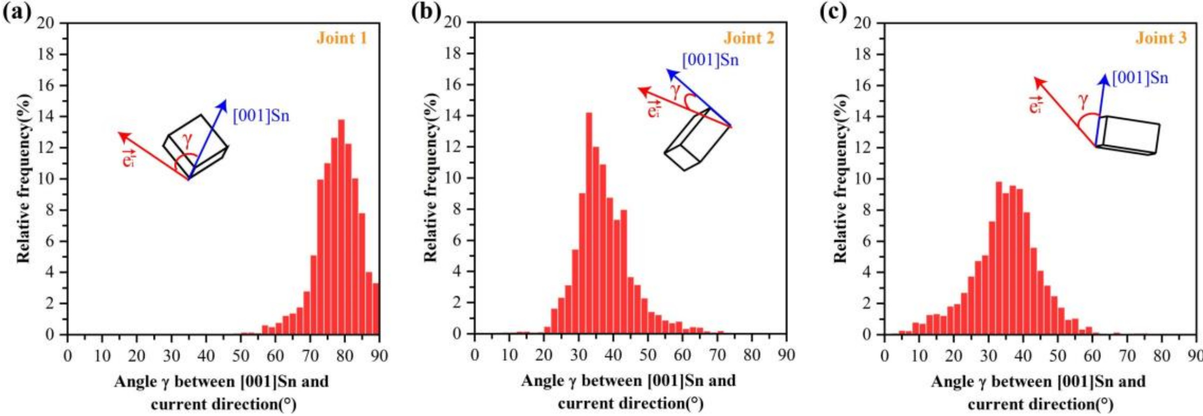

Figure 15. The distribution of the angle γ between [001]Sn and the current direction [29].

Bi, as an environmentally friendly green element with a low cost, can be used as an alloying element to enhance the performance of SAC305. This not only contributes to environmental protection but also reduces production costs. Additionally, by comparing it with the addition of elements such as Zn, In, Ni, and Co [8,10,11,31] from other studies, the potential optimization directions for SAC305 solder can be further refined.

4. Conclusions

With the addition of Bi, the ultimate tensile strength and microhardness of the SAC305 solder alloy initially increase and then decrease. When the content of Bi was 0.5%, the alloy showed the highest ultimate tensile strength and microhardness. However, the fracture strain first decreased gradually and then decreased sharply. When the content of Bi was 0.5% and 0.75%, the ultimate tensile strength of the SAC305 alloy enhanced and it also maintained good plasticity.

The wettability of SAC305-*x*Bi solder alloys initially increased and then decreased with the addition of Bi. When the content of Bi was 0.5%, the wettability was at its best, and the solder alloy demonstrated the largest spreading area and the smallest wetting angle.

After the EM experiment of SAC305-*x*Bi solder alloys, two kinds of IMCs, Cu_6Sn_5 and Cu_3Sn, formed at the interface between the anode and cathode. The addition of Bi had little effect on the growth of IMC at the anode interface during EM of the SAC305 solder alloy, and the total thickness of IMC at the anode interface of the alloy containing Bi was not much different from SAC05 at the same EM experiment time. However, the addition of Bi notably inhibited the reduction in the total thickness of IMC at the cathode interface; in particular, when the content of Bi was 0.75%, the inhibition effect was the most prominent and the EM performance was improved.

Through this study, we found that adding trace amounts of Bi to SAC305 can enhance its electromigration resistance, while also improving its mechanical properties and wettability to some extent compared to the SAC305 alloy. Therefore, when optimizing the performance of the SAC305 alloy or developing the next generation of lead-free solder, Bi can be considered as an additive alloy. Due to the limited research methods in this paper and the trace amounts of Bi added, the effects of higher Bi content in the alloy, especially when the Bi content exceeds 1 wt.%, which leads to a decline in both mechanical properties and electromigration resistance, require further investigation.

Author Contributions: Conceptualization, Z.X.; Methodology, H.Z. and Z.X.; Formal analysis, Y.W.; Investigation, Y.W.; Resources, Z.X., C.F., S.M. and J.Y.; Data curation, H.Z.; Writing–original draft, H.Z.; Supervision, C.T. All authors have read and agreed to the published version of the manuscript.

Funding: This study was funded by the Natural Science Foundation of Hebei Province (E2020203158, E2022203182), Science and Technology Plan Project of Hebei Academy of Sciences (24704), the High level Talent Support Project of Hebei Province (E2020100006), the Innovation Ability Enhancement Project of Hebei Province (22567609H), and the National Natural Science Foundation of China (52173231).

Data Availability Statement: The original contributions presented in the study are included in the article, further inquiries can be directed to the corresponding author.

Conflicts of Interest: The authors declare no conflict of interest.

References

1. Shanthi Bhavan, J.; Pazhani, A.; Unnikrishnan, T.G. EBSD characterization of Ag3Sn phse transformation in Sn–Ag lead-free solder alloys: A comparative study before and after heat treatment. *J. Mater. Sci. Mater. Electron.* **2024**, *35*, 1577. [CrossRef]
2. Huang, H.; Chen, B.; Hu, X.; Jiang, X.; Li, Q.; Che, Y.; Zu, S.; Liu, D. Research on Bi contents addition into Sn–Cu-based lead-free solder alloy. *J. Mater. Sci. Mater. Electron.* **2022**, *33*, 15586–15603. [CrossRef]
3. Gerhátová, Ž.; Babincová, P.; Drienovský, M.; Pašák, M.; Černičková, I.; Ďuriška, L.; Havlík, R.; Palcut, M. Microstructure and Corrosion Behavior of Sn–Zn Alloys. *Materials* **2022**, *15*, 7210. [CrossRef] [PubMed]
4. Hu, T.; Li, S.; Li, Z.; Wu, G.; Zhu, P.; Dong, W.; Sun, Y.; Zhou, J.; Wu, B.; Zhao, B.; et al. Coupled effect of Ag and In addition on the microstructure and mechanical properties of Sn–Bi lead-free solder alloy. *J. Mater. Res. Technol.* **2023**, *26*, 5902–5909. [CrossRef]
5. Kang, Y.; Choi, J.J.; Kim, D.G.; Shim, H.W. The Effect of Bi and Zn Additives on Sn-Ag-Cu Lead-Free Solder Alloys for Ag Reduction. *Metals* **2022**, *12*, 1245. [CrossRef]
6. Noh, E.C.; Seo, Y.J.; Yoon, J.W. Effects of solder ball size and reflow cycles on properties of Sn-3.0Ag-0.5Cu/Cu joints. *J. Mater. Sci. Mater. Electron.* **2023**, *34*, 2176. [CrossRef]
7. Yin, S.Q.; Ren, J.; Huang, M.L. Electromigration behavior of Sn–3.0Ag–0.5Cu/Sn–37Pb hybrid solder joints with various mixed percentages for aerospace electronics. *J. Mater. Sci. Mater. Electron.* **2024**, *35*, 838. [CrossRef]
8. Han, J.; Cao, H.; Meng, Z.; Jin, X.; Ma, L.; Guo, F.; An, T.; Wang, T. Study on Electromigration Mechanism of Lead-Free Sn3.5Ag0.5Bi8.0In Solder Joints. *J. Electron. Mater.* **2023**, *52*, 1216–1232. [CrossRef]
9. Li, M.; Zhang, L.; Jiang, N.; Zhang, L.; Zhong, S.-J. Materials modification of the lead-free solders incorporated with micro/nano-sized particles: A review. *Mater. Des.* **2021**, *197*, 109224. [CrossRef]
10. Ma, L.; Xu, G.; Sun, J.; Guo, F.; Wang, X. Effects of Co additions on electromigration behaviors in Sn–3.0 Ag–0.5 Cu-based solder joint. *J. Mater. Sci.* **2011**, *46*, 4896–4905. [CrossRef]
11. Bashir, M.N.; Khan, A.F.; Bashir, S.; Bashir, M.B.A.; Jamshaid, M.; Javed, I.; Ali, I. Effect of Zn nanoparticle doped flux on electromigration damages in SAC305 solder joint. *J. Mater. Sci. Mater. Electron.* **2023**, *34*, 351. [CrossRef]
12. Kim, Y.; Nagao, S.; Sugahara, T.; Suganuma, K.; Ueshima, M.; Albrecht, H.J.; Wilke, K.; Strogies, J. Enhanced reliability of Sn–Ag–Bi–In joint under electric current stress by adding Co/Ni elements. *J. Mater. Sci. Mater. Electron.* **2014**, *25*, 3090–3095. [CrossRef]
13. Sun, F.L.; Wang, J.B.; Liu, Y.; Wang, G.J. Electromigration of SnAgCu-Bi-Ni Pb-free Micro Solder Joints. *J. Harbin Univ. Sci. Technol.* **2012**, *17*, 1–4. (In Chinese)
14. Wang, Y.; Han, J.; Ma, L.; Zuo, Y.; Guo, F. Electromigration behaviors of Cu reinforced Sn-3.5Ag composite solder joints. *J. Electron. Mater.* **2016**, *45*, 6095–6101. [CrossRef]
15. Liang, Y.C.; Tsao, W.A.; Chen, C.; Yao, D.J.; Huang, A.T.; Lai, Y.S. Influence of Cucolumn under-bump-metallizations on currentcrowding and Joule heating effects of electromigra-tion inflip-chip solder joints. *J. Appl. Phys.* **2012**, *111*, 043705. [CrossRef]
16. Wang, C.; Shen, H.; Lai, W. Effective suppression of electromigration-induced Cu dissolution by using Ag as a barrier layer in lead-free solder joints. *J. Alloys Compd.* **2013**, *564*, 35–41. [CrossRef]
17. Long, Z.; Liu, S.; Liu, L.; Tan, Y.; Wang, Z.; Wang, X. Microstructure refinement, thermodynamic characteristic, wettability and shear strength of Bi-added rapid solidification SAC305 solder. *J. Mater. Sci. Mater. Electron.* **2022**, *33*, 8016–8026. [CrossRef]
18. Chen, W.J.; Lee, Y.L.; Wu, T.Y.; Chen, T.C.; Hsu, C.H.; Lin, M.T. Effects of Electrical Current and External Stress on the Electromigration of Intermetallic Compounds Between the Flip-Chip Solder and Copper Substrate. *J. Electron. Mater.* **2018**, *47*, 35–48. [CrossRef]
19. Ren, X.; Wang, Y.-P.; Lai, Y.-Q.; Shi, S.-Y.; Liu, X.-Y.; Zou, L.-J.; Zhao, N. Effects of In addition on microstructure and properties of SAC305 solder. *Trans. Nonferrous Met. Soc. China* **2023**, *33*, 3427–3438. [CrossRef]
20. Tu, X.; Yi, D.; Wu, J.; Wang, B. Influence of Ce addition on Sn-3.0Ag-0.5Cu solder joints: Thermal behavior, microstructure and mechanical properties. *J. Alloys Compd.* **2017**, *698*, 317–328. [CrossRef]
21. Kang, H.; Rajendran, S.H.; Jung, J.P. Low Melting Temperature Sn-Bi Solder: Effect of Alloying and Nanoparticle Addition on the Microstructural, Thermal, Interfacial Bonding, and Mechanical Characteristics. *Metals* **2021**, *11*, 364. [CrossRef]

22. Yin, L.; Zhang, Z.; Su, Z.; Zhang, H.; Zuo, C.; Yao, Z.; Wang, G.; Zhang, L.; Zhang, Y. Interfacial microstructure evolution and properties of Sn-0.3Ag-0.7Cu–xSiC solder joints. *Mater. Sci. Eng. A* **2021**, *809*, 140995. [CrossRef]
23. Qu, M.; Cao, T.; Cui, Y.; Liu, F.; Jiao, Z. Effect of nano-ZnO particles on wettability, interfacial morphology and growth kinetics of Sn–3.0Ag–0.5Cu–xZnO composite solder. *J. Mater. Sci. Mater. Electron.* **2019**, *30*, 19214–19226. [CrossRef]
24. Bashir, M.N.; Butt, S.U.; Mansoor, M.A.; Khan, N.B.; Bashir, S.; Wong, Y.H.; Alamro, T.; Eldin, S.M.; Jameel, M. Role of Crystallographic Orientation of β-Sn Grain on Electromigration Failures in Lead-Free Solder Joint: An Overview. *Coatings* **2022**, *12*, 1752. [CrossRef]
25. Chantaramanee, S.; Sungkhaphaitoon, P. Influence of bismuth on microstructure, thermal properties, mechanical performance, and interfacial behavior of SAC305-xBi/Cu solder joints. *Trans. Nonferrous Met. Soc. China* **2021**, *31*, 1397–1410. [CrossRef]
26. Laurila, T.; Vuorinen, V.; Kivilahti, J.K. Interfacial reactions between lead-free solders and common base materials. *Mater. Sci. Eng. R Rep.* **2005**, *49*, 1–60. [CrossRef]
27. Huang, T.; Yang, T.; Ke, J.; Hsueh, C.; Kao, C. Effects of Sn grain orientation on substrate dissolution and intermetallic precipitation in solder joints under electron current stressing. *Scr. Mater.* **2014**, *80*, 37–40. [CrossRef]
28. Dyson, B.F. Diffusion of gold and silver in tin single crystals. *J. Appl. Phys.* **1966**, *37*, 2375–2377. [CrossRef]
29. Li, C.; Yuan, H.; Ma, Z.; Cheng, X. Effect of βSn grain orientations on the electromigration-induced evolution of voids in SAC305 BGA solder joints. *Mater. Charact.* **2024**, *215*, 114227. [CrossRef]
30. Zhao, J.; Cheng, C.-Q.; Qi, L.; Chi, C.-Y. Kinetics of intermetallic compound layers and shear strength in Bi-bearing SnAgCu/Cu soldering couples. *J. Alloys Compd.* **2009**, *473*, 382–388. [CrossRef]
31. Liu, Y.; Li, S.; Zhang, H.; Cai, H.; Sun, F.; Zhang, G. Microstructure and hardness of SAC305-xNi solder on Cu and graphene-coated Cu substrates. *J. Mater. Sci. Mater. Electron.* **2018**, *29*, 13167–13175. [CrossRef]

Disclaimer/Publisher's Note: The statements, opinions and data contained in all publications are solely those of the individual author(s) and contributor(s) and not of MDPI and/or the editor(s). MDPI and/or the editor(s) disclaim responsibility for any injury to people or property resulting from any ideas, methods, instructions or products referred to in the content.